

Erratum: The Tidal Tails of 47 Tucanae

Richard R. Lane^{1*}, Andreas H.W. Küpper^{2,3} and Douglas C. Heggie⁴

¹*Departamento de Astronomía, Universidad de Concepción, Casilla 160 C, Concepción, Chile*

²*Argelander-Institut für Astronomie (AIfA), Auf dem Hügel 71, 53121 Bonn, Germany*

³*European Southern Observatory, Alonso de Cordova 3107, Vitacura, Santiago, Chile*

⁴*University of Edinburgh, School of Mathematics and Maxwell Institute for Mathematical Sciences, King’s Buildings, Edinburgh EH9 3JZ, U.K.*

Accepted..... Received.....; in original form.....

Key words: Galaxy: globular clusters: general – Galaxy: globular clusters: individual: 47 Tucanae – Galaxy: kinematics and dynamics – methods: numerical

Table 1. Revised orbital parameters of the reference model

Parameter	Value
Edge radius	142 pc
Minimum orbital velocity	179 km s ⁻¹
Maximum orbital velocity	254 km s ⁻¹
Current orbital velocity	184 km s ⁻¹
Apocentre	7.65 kpc
Pericentre	6.10 kpc
Current Galactocentric distance	7.60 kpc
Orbital eccentricity	0.11
Orbital phase	+0.97

The paper “The Tidal Tails of 47 Tucanae” was published in Mon. Not. R. Astron. Soc. 423, 2845 (2012). An error was discovered, which affected the results reported in that paper. This error is corrected here.

We used, for our proper motion of 47 Tucanae (47 Tuc), the values published by Anderson & King (2004), however, we incorrectly adjusted the published values of μ_α by $\cos \delta$. These values were already published with the $\cos \delta$ included so this was unnecessary. Our new reference model for this erratum uses proper motions:

$$\mu_\alpha \cos \delta = 5.64 \text{ mas yr}^{-1} \quad (1)$$

$$\mu_\delta = -2.05 \text{ mas yr}^{-1} \quad (2)$$

All other input parameters were correct and are left unchanged. All references for, and reasons behind, our choices for the input parameters can be found in the original paper. The newly computed models are presented in the following.

1 THE ORBIT

The last 500 Myr of the (x,y) and (x,z) orbital paths of 47 Tuc derived from the new proper motion and radial velocity of the cluster are shown in Figure 1. Due to the signif-

icant change in proper motion, various orbital parameters have been altered. The new quantities, defined as per the original paper, are listed in Table 1. We particularly note that (for our choice of Galaxy model) the orbit of 47 Tuc is less eccentric than originally thought ($\epsilon = 0.11$) and that 47 Tuc is very close to reaching the apocentre of its orbit ($p_{orb} = +0.97$).

2 THE TIDAL TAILS

Figures 2-8 in this erratum are based on our new models, and correspond to Figures 3-9 from the original paper. Table 2 summarises our corrected results. Qualitatively, the results are effectively equivalent, but the shape of the tidal tails and, therefore, the positions of their overdensities have changed.

!
!
!
!
!
!
!
!
!
!

ACKNOWLEDGMENTS

The authors gratefully thank Radek Poleski for bringing the error to our attention.

REFERENCES

Anderson, J., & King, I. R. 2004, AJ, 128, 950
 Lane, R. R., Küpper, A. H. W., & Heggie, D. C. 2012, MNRAS, 423, 2845

* E-mail: rlane@astro-udec.cl (RRL); akuepper@astro.uni-bonn.de (AHWK); dcheggie@ed.ac.uk (DCH)

Table 2. The density and Galactic coordinates of the first and second order overdensities, the proper motion, final (present day) cluster mass, Heliocentric distance and escape conditions for each of our corrected models. Only the trailing tail is represented here for brevity. Information is for the peak density in each overdensity only. Note that the approximate average density of the stellar background in the regions of the first and second tidal overdensities is 3000 stars per square degree, based on 2MASS point sources.

Model	Σ_1 ★/deg ²	Σ_2 ★/deg ²	(l,b) ₁ deg	(l,b) ₂ deg	$\mu_\alpha \cos \delta$ mas yr ⁻¹	μ_δ mas yr ⁻¹	$\times 10^6$ M _⊙	D kpc	Esc
1	85	115	(-60.4,-34.5)	(-56.7,-26.5)	5.64	-2.05	1.0	4.02	warm
2	55	70	(-60.5,-34.5)	(-57.0,-29.2)	5.64	-2.05	1.0	4.02	hot
3	120	110	(-56.5,-34.9)	(-52.2,-27.7)	7.05	-2.05	1.0	4.02	warm
4	100	100	(-62.0,-38.7)	(-61.6,-31.0)	4.23	-2.05	1.0	4.02	warm
5	85	110	(-56.5,-28.0)	(-69.2,-33.6)	5.64	-2.56	1.0	4.02	warm
6	95	130	(-60.3,-34.0)	(-56.9,-24.7)	5.64	-1.54	1.0	4.02	warm
7	85	120	(-60.4,-34.3)	(-56.5,-25.5)	5.64	-2.05	1.1	4.02	warm
8	95	130	(-60.2,-35.0)	(-57.0,-27.0)	5.64	-2.05	0.9	4.02	warm
9	65	85	(-63.7,-32.6)	(-60.4,-23.5)	5.64	-2.05	1.0	3.30	warm
10	120	125	(-57.7,-35.7)	(-53.7,-29.0)	5.64	-2.05	1.0	4.70	warm

This paper has been typeset from a \TeX / \LaTeX file prepared by the author.

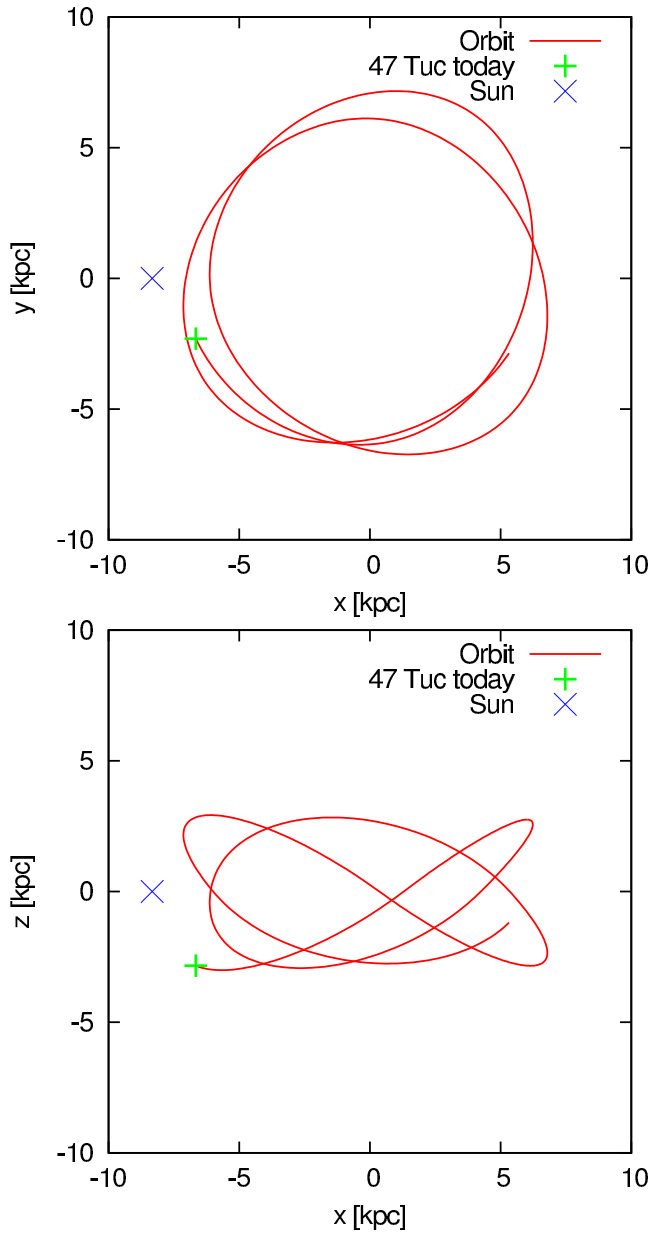


Figure 1. The orbital path of 47 Tuc from 500 Myr ago to the present time in the (x, y) plane (top panel) and in the (x, z) plane (bottom panel), based on parameters from the corrected proper motions (see text). The present day position of 47 Tuc is marked as a plus (+) symbol and the position of the Sun is marked as a cross (x). Corresponds to Figure 2 of the original paper.

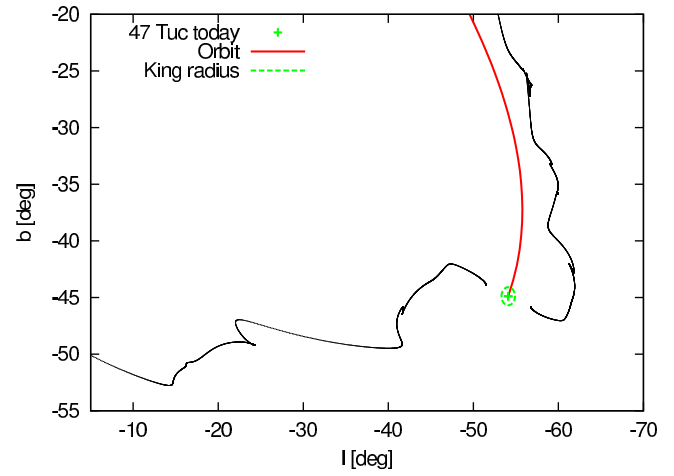


Figure 2. The final timestep for the reference model. Corresponds to Figure 3 from the original paper.

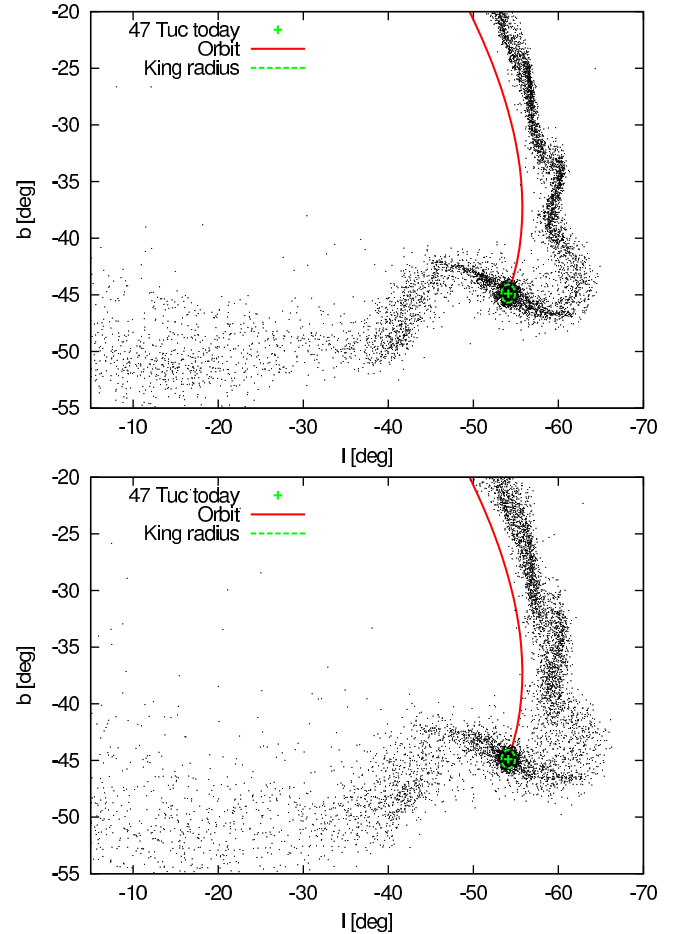


Figure 3. Same as Figure 2 except with warm (top) and hot (bottom) escape conditions. Corresponds to Figure 4 of the original paper.

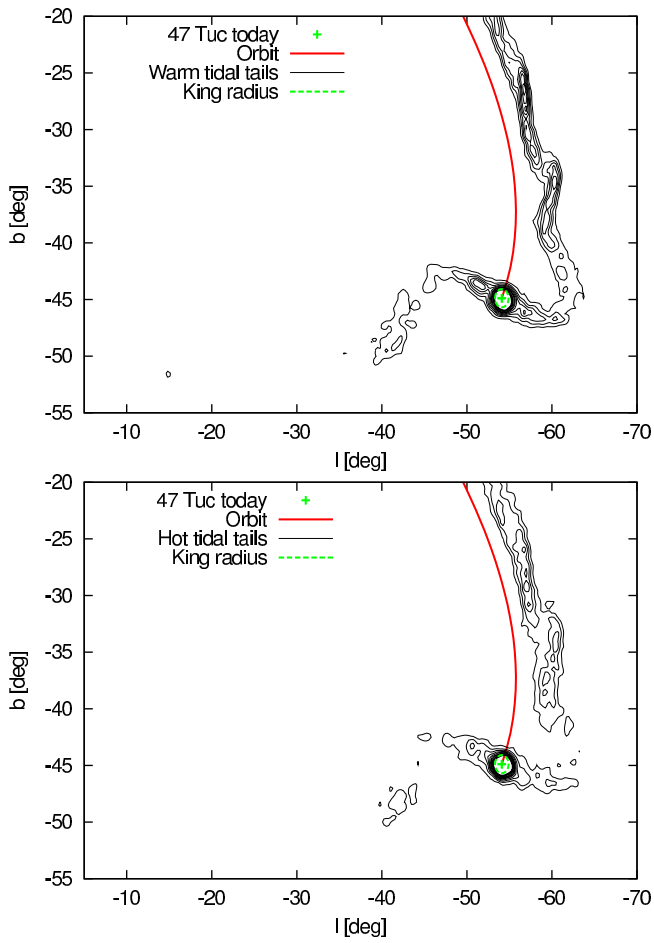


Figure 4. Contour representation of Figure 3 with “warm” escape conditions in the top panel and “hot” escape conditions in the bottom panel. Corresponds to Figure 5 of the original paper.

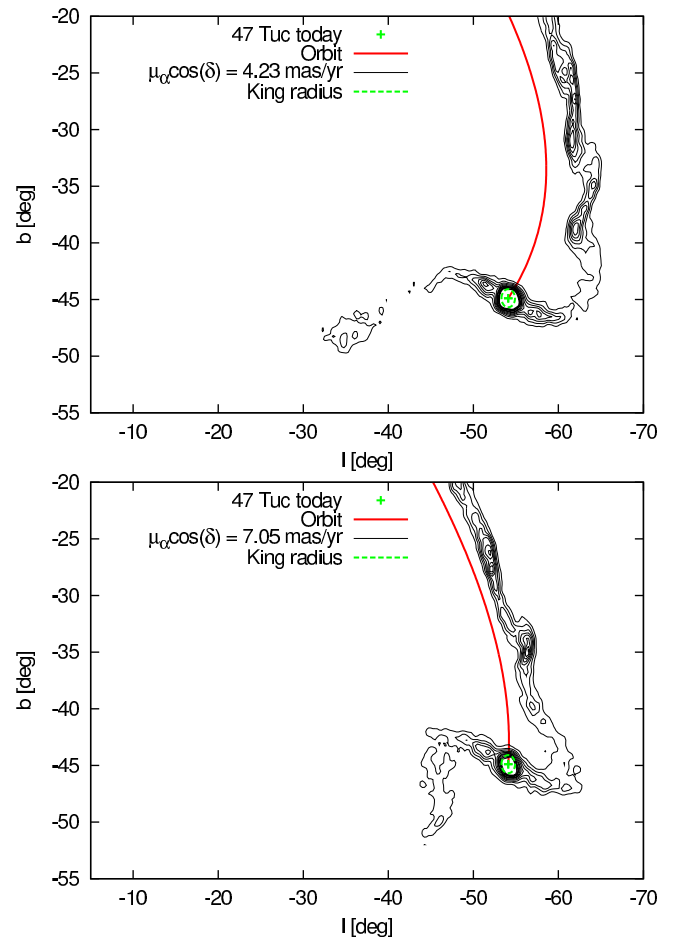


Figure 5. Same as for the top panel of Figure 4, except with $\mu_\alpha \cos \delta = 4.23 \text{ mas yr}^{-1}$ (top panel) and $\mu_\alpha \cos \delta = 7.05 \text{ mas yr}^{-1}$ (bottom panel). Corresponds to Figure 6 of the original paper.

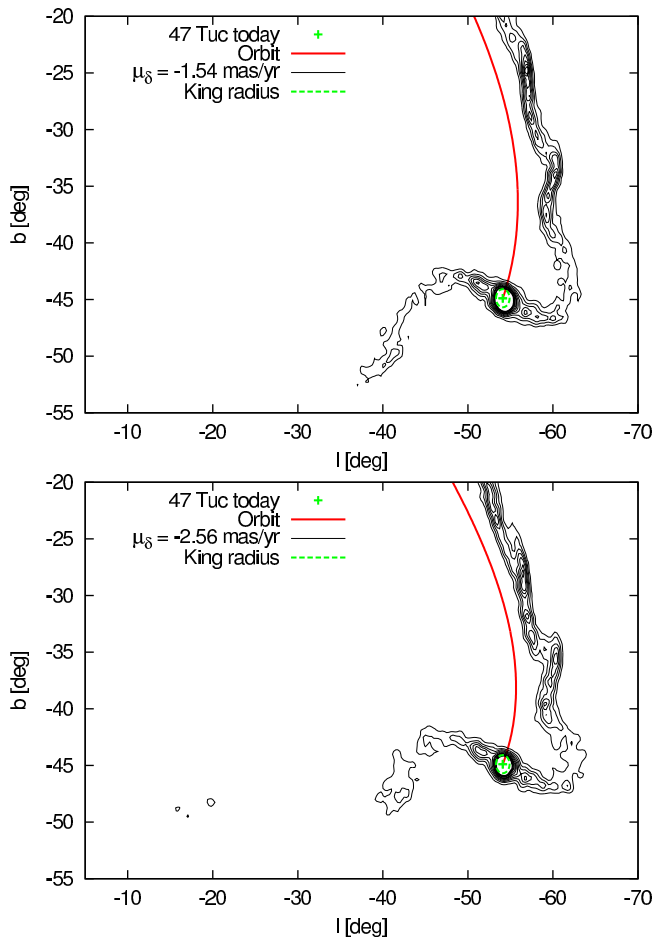


Figure 6. Same as for the top panel of Figure 4, except with $\mu_\delta = -1.54 \text{ mas yr}^{-1}$ (top panel) and $\mu_\delta = -2.56 \text{ mas yr}^{-1}$ (bottom panel). Corresponds to Figure 7 of the original paper.

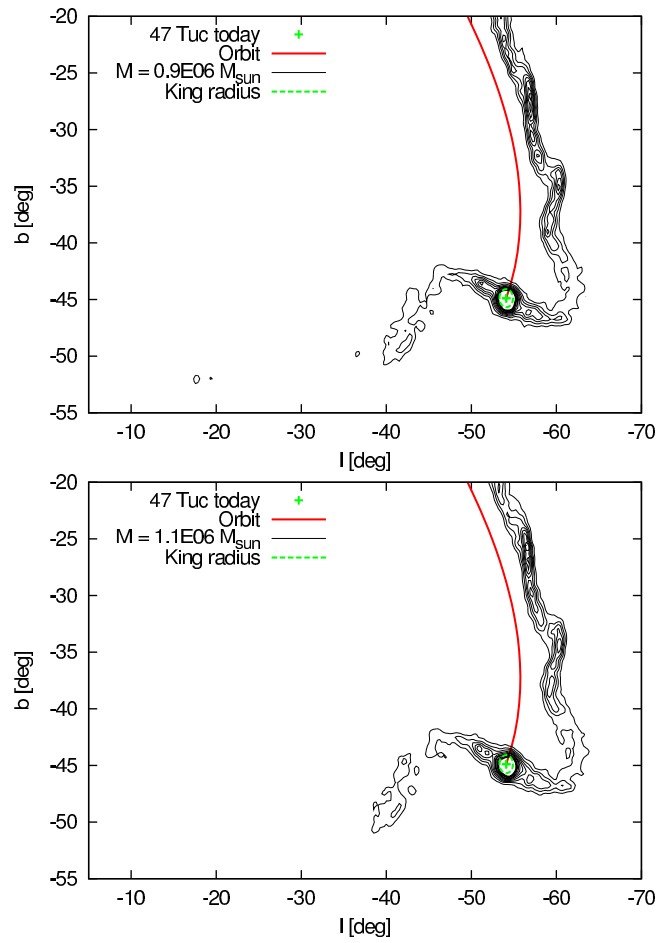


Figure 7. Same as for the top panel of Figure 4, except with $M = 0.9 \times 10^6 M_\odot$ (top panel) and $M = 1.1 \times 10^6 M_\odot$ (bottom panel). Corresponds to Figure 8 of the original paper.

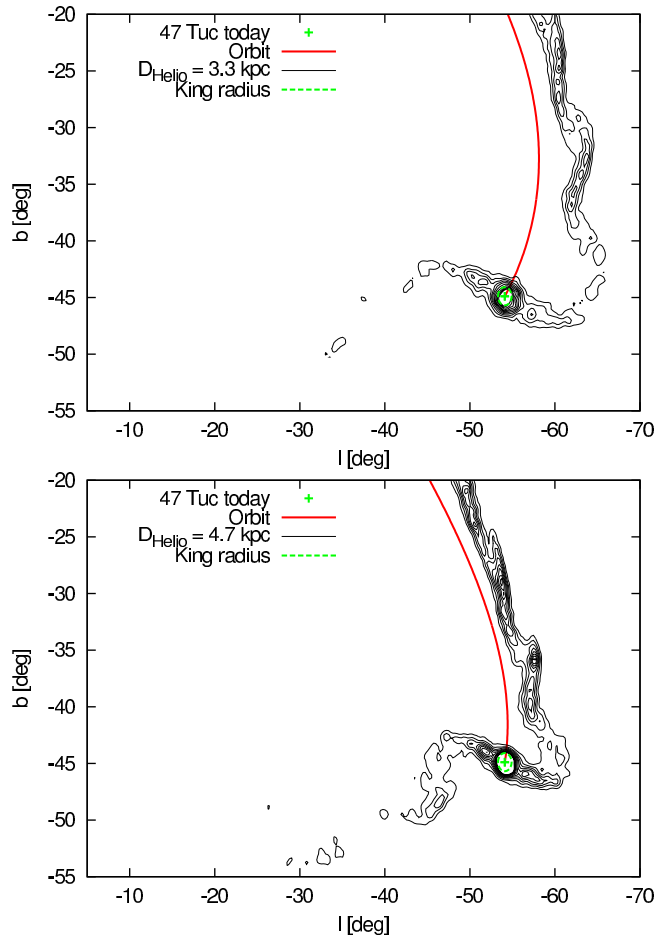


Figure 8. Same as for the top panel of Figure 4, except with $D_{\text{helio}} = 3.3$ kpc (top panel) and $D_{\text{helio}} = 4.7$ kpc (bottom panel). Corresponds to Figure 9 of the original paper.

The Tidal Tails of 47 Tucanae

Richard R. Lane^{1*}, Andreas H.W. Küpper^{2,3} and Douglas C. Heggie⁴

¹*Departamento de Astronomía, Universidad de Concepción, Casilla 160 C, Concepción, Chile*

²*Argelander-Institut für Astronomie (AIfA), Auf dem Hügel 71, 53121 Bonn, Germany*

³*European Southern Observatory, Alonso de Cordova 3107, Vitacura, Santiago, Chile*

⁴*University of Edinburgh, School of Mathematics and Maxwell Institute for Mathematical Sciences, King's Buildings, Edinburgh EH9 3JZ, U.K.*

Accepted..... Received.....; in original form.....

ABSTRACT

The Galactic globular cluster 47 Tucanae (47 Tuc) shows a rare increase in its velocity dispersion profile at large radii, indicative of energetic, yet bound, stars at large radii dominating the velocity dispersion and, potentially, of ongoing evaporation. Escaping stars will form tidal tails, as seen with several Galactic globular clusters, however, the tidal tails of 47 Tuc are yet to be uncovered. We model these tails of 47 Tuc using the most accurate input data available, with the specific aim of determining their locations, as well as the densities of the epicyclic overdensities within the tails. The overdensities from our models show an increase of 3-4% above the Galactic background and, therefore, should be easily detectable using matched filtering techniques. We find that the most influential parameter with regard to both the locations and densities of the epicyclic overdensities is the Heliocentric distance to the cluster. Hence, uncovering these tidal features observationally will contribute greatly to the ongoing problem of determining the distance to 47 Tuc, tightly constraining the distance of the cluster independent of other methods. Using our streakline method for determining the locations of the tidal tails and their overdensities, we show how, in principle, the shape and extent of the tidal tails of any Galactic globular cluster can be determined without resorting to computationally expensive N -body simulations.

Key words: Galaxy: globular clusters: general – Galaxy: globular clusters: individual: 47 Tucanae – Galaxy: kinematics and dynamics – methods: numerical

1 INTRODUCTION

47 Tucanae (47 Tuc) is among the most interesting and best studied globular clusters of the Milky Way (MW). It is one of the most massive, and exhibits some peculiar properties, including a recently detected rise in the velocity dispersion at large cluster radii (Lane et al. 2010a). Such a rise in the velocity dispersion profile of a globular cluster was first noted some time ago by Drukier et al. (1998) in M15. While a rise of this nature is intuitively unexpected for a velocity dispersion profile in Newtonian dynamics, it arises naturally in modified gravitational theories like MOND (e.g. Scarpa & Falomo 2010).

In the case of 47 Tuc Lane et al. (2010b) posed, as an alternative explanation for this phenomenon, the existence of two separate kinematic populations, a relic of its formation. A third explanation was suggested more recently by Küpper et al. (2010b), who found a similar rise in velocity dispersion in their N -body models of star clusters orbit-

ing in galactic tidal fields. Their alternate explanation arises from the contribution of energetically unbound stars which haven't yet escaped the cluster potential. These "potential escapers" of Küpper et al. (2010b) are preferentially located at larger radii, where they dominate the velocity dispersion. Moreover, they are an indicator of ongoing, relaxation driven mass loss (evaporation), since a star has to become a potential escaper before it eventually escapes from the cluster to become a member of the tidal tails (Fukushige & Heggie 2000; Küpper et al. 2010b). Dynamically cold tidal tails emanating from 47 Tuc are, therefore, to be expected in this scenario. Hence, locating these tails will help to clarify the mechanism responsible for rising velocity dispersion profiles in globular clusters.

Tidal streams formed in this way have been observed for other MW globular clusters like Palomar 5 and NGC 5466 (Odenkirchen et al. 2003; Grillmair & Johnson 2006), but no tidal tails associated with 47 Tuc have yet been uncovered. However, Lane et al. (2010a) found 25 stars outside the tidal radius given in the Harris (1996) catalogue, possible evidence for evaporation. Furthermore, these apparently extra-tidal stars precisely follow the trend of increased veloc-

* E-mail: rlane@astro-udec.cl (RRL); akuepper@astro.uni-bonn.de (AHWK); dcheggie@ed.ac.uk (DCH)

ity dispersion as found by Küpper et al. (2010b) in N -body computations (see Fig. 11 by Lane et al. 2010a).

The lack of prominent extra-tidal features could be due to the non-linear motion of stars within tidal tails. Küpper et al. (2008) and Just et al. (2009) found that the epicyclic motion of evaporating stars results in periodic over- and underdensities within the tidal tails, even if they are formed by a constant stream of escaping stars. The periodicity is spatial, meaning that the overdensities are regularly spaced, at least in the case of a circular galactic orbit, and are found in both the leading and trailing tails. Their spatial separation equates to the distance through which an escaper drifts (relative to the cluster) in one epicyclic period, and decreases slowly as the cluster loses mass. Close to the tidal radius the escaping stars are accelerated away from the cluster, therefore, this motion leads to a pronounced underdensity of stars close to the cluster. Hence, most clusters should not exhibit extended tidal features, but rather a steeply decreasing surface brightness close to the cluster (e.g. see Fig. 1). The epicyclic overdensities, on the other hand, can reach surface densities several times higher than the average density within the tidal tails, but are typically located many tidal radii from the cluster and thus the association with the cluster may not be obvious. The positions of these overdensities can be accurately predicted, however, if the dynamical state of the cluster (i.e. its orbit, location & mass) is sufficiently constrained (Küpper et al. 2010a; Küpper, Lane & Heggie 2012).

Since the orbit of 47 Tuc has been determined in a number of observational studies, and it has been subject to extensive numerical modelling, its dynamical state is thought to be well understood. Thus, our knowledge of 47 Tuc provides an opportunity for predicting and finding the overdensities in its tidal tails and, therefore, constraining the dynamical state of 47 Tuc independently from other methods. Moreover, the detection of the overdensities in the tails of 47 Tuc will shed light on the consistency of our theoretical understanding of Newtonian gravity.

This work is organised as follows: based on the most accurate data available (Sec. 2), we calculate the orbital parameters of 47 Tuc and predict the shape of its tidal tails and, most importantly, the positions and extents of the epicyclic overdensities (Sec. 3). Finally we give a short summary and conclusions in Sec. 4.

2 INPUT DATA

For this work we require accurate input data to ensure the best quality orbital model (see Table 1 for a summary). For this reason we have chosen to take our positional information from McLaughlin et al. (2006) who claim a nearly complete, uniform sample of all stars within 1.5 (~ 5 core radii) of the cluster centre, which the authors calculate to be at (RA,dec)=($00^{\text{h}}24^{\text{m}}05^{\text{s}}.67 \pm 0^{\text{s}}.07$, $-72^{\circ}04'52''.62 \pm 0''.26$). We also take our Heliocentric distance information from McLaughlin et al. (2006), who calculate a kinematic distance of 4.02 ± 0.35 kpc by comparing the velocity dispersion of stars within the inner $\sim 105''$ with the proper motions in the same region to estimate a distance to the cluster.

For our proper motion we use the values derived by Anderson & King (2004), who used *Hubble Space Telescope*

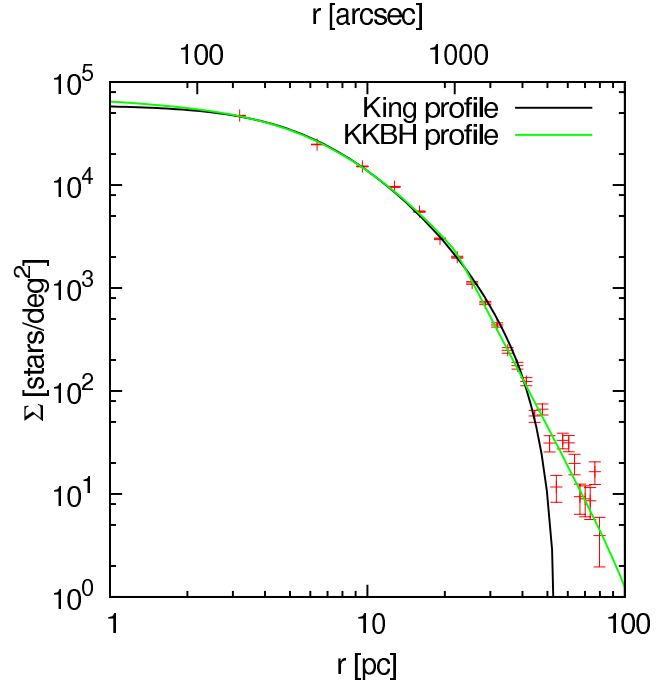


Figure 1. Surface density profile of 47 Tuc based on data from Lane et al. (2010a), overlaid with a King profile (King 1962, solid black curve) and a KKBH profile (Küpper et al. 2010b, solid green curve). The radius where the surface density drops to zero is 56 pc in the case of the King profile. The cut-off radius of the core of the KKBH profile is slightly larger (65 pc). However, the power-law component of the KKBH extends out to the last data point with a slope of -4.8 .

(*HST*) data to find the proper motion of 47 Tuc to be 5.64 ± 0.20 mas yr $^{-1}$ in RA and -2.05 ± 0.20 mas yr $^{-1}$ in dec. These data are considered the best available data for the current work because the Small Magellanic Cloud is in the same line of sight as 47 Tuc, allowing the authors to obtain very accurate differential proper motions. Indeed they claim an order of magnitude greater accuracy than previous studies.

We have chosen to use the radial velocity of -16.85 ± 0.16 km s $^{-1}$ derived by Lane et al. (2010a) from the largest known spectroscopic GC study to date. Their survey of ~ 2200 individual spectra of stellar members provides the most accurately determined radial velocity to date. The surface density profile from the Lane et al. (2010a) dataset can be seen in Fig. 1. Note that the King model fit is excellent out to large radius (where the influence from the potential escapers becomes important, and apparent) and the King tidal radius from the fit is in excellent agreement to that given by the Harris (1996) catalogue. Fitting a KKBH profile (Küpper et al. 2010b) to the same data yields a slightly larger cut-off radius for the core profile (65 pc) and a power-law slope of -4.8 at large cluster radii. As we show later, the stars at radii larger than the cut-off radius are not extra-tidal. The theoretical tidal radius of 47 Tuc is larger than the range of the data (see Sec. 3), so the fitted cut-off radii are both well inside the tidal sphere. Hence, the surface density profile does not show a clear cut-off at about 60 pc, but continues with a constant power-law slope. Extra-tidal signatures like tidal distortions are only expected at much larger radii of a few hundred parsecs (e.g. see Fig. 4).

To estimate surface densities in the modelled tidal tails and their epicyclic overdensities, it is important to have an independently derived mass-loss rate for the cluster. Using detailed Monte Carlo models of the dynamical evolution of 47 Tuc, Giersz & Heggie (2011) found an escape rate of 13.9 stars per Myr, with an average stellar mass of $0.404 M_{\odot}$, giving a mass loss rate of $5.61 M_{\odot} \text{ Myr}^{-1}$. We have adopted their value here.

Many studies exist with measurements of the total mass of 47 Tuc, however, the most recent of these, Lane et al. (2010a) and Giersz & Heggie (2011), based on observations and numerical modelling, respectively, find masses of $1.1 \times 10^6 M_{\odot}$ and $0.9 \times 10^6 M_{\odot}$ which are in remarkable agreement. We have, therefore, chosen $1.0 \times 10^6 M_{\odot}$ as the baseline mass for our models.

The Solar galactocentric distance we take from Gillessen et al. (2009) who find $R_0 = 8.33 \pm 0.35 \text{ kpc}$ by fitting orbits to stars associated with the Galactic centre. Since the distance to the Galactic centre strongly correlates with the mass of the central black hole (see Fig. 15 by Gillessen et al. 2009) these orbital fits tightly constrain the distance to the Galactic centre, independent of other methodologies.

In a review of twenty independent measurements of the Solar circular velocity dating back to 1974, Kerr & Lynden-Bell (1986) concluded that a case can be made for accepting the IAU standard value of 220 km s^{-1} , since the mean value of these twenty studies is 222.2 km s^{-1} . We have, therefore, chosen to use the IAU standard of 220 km s^{-1} for the current study (see also Koposov, Rix & Hogg 2010, who find $V_c = 224 \pm 13 \text{ km s}^{-1}$, in agreement with the IAU standard).

For the Local Standard of Rest we are adopting $(U, V, W)_{\text{LSR}} = (11.1^{+0.69}_{-0.75}, 12.24^{+0.47}_{-0.47}, 7.25^{+0.37}_{-0.36}) \text{ km s}^{-1}$ by Schönrich et al. (2010) as this is the only study to take into account the metallicity gradient in the Galactic disc. Without adjusting for this gradient, the V component is significantly affected due to the correlation between stellar group colours and the radial gradients of their properties.

The coordinates of the Galactic North Pole, which are required for coordinate and proper motion transformations, we take from Reid & Brunthaler (2004). All input data are summarised in Table 1.

3 RESULTS

Using the input data described in the previous section, we first derive the orbit of 47 Tuc about the Galactic centre by means of numerical integration. We then use this orbit to apply the method described by Küpper, Lane & Heggie (2012) for predicting the shape of the tidal tails of the cluster. Finally we discuss the epicyclic overdensities within those tails.

3.1 The orbit

The last 500 Myr of the (x, y) and (x, z) orbital paths of 47 Tuc derived from the proper motion and radial velocity of the cluster (see Table 1) are shown in Fig. 2. For this purpose we integrated the cluster orbit, assuming the Milky Way potential suggested by Allen & Santillan (1991), consisting of a central point mass, a disc and an isothermal halo. This

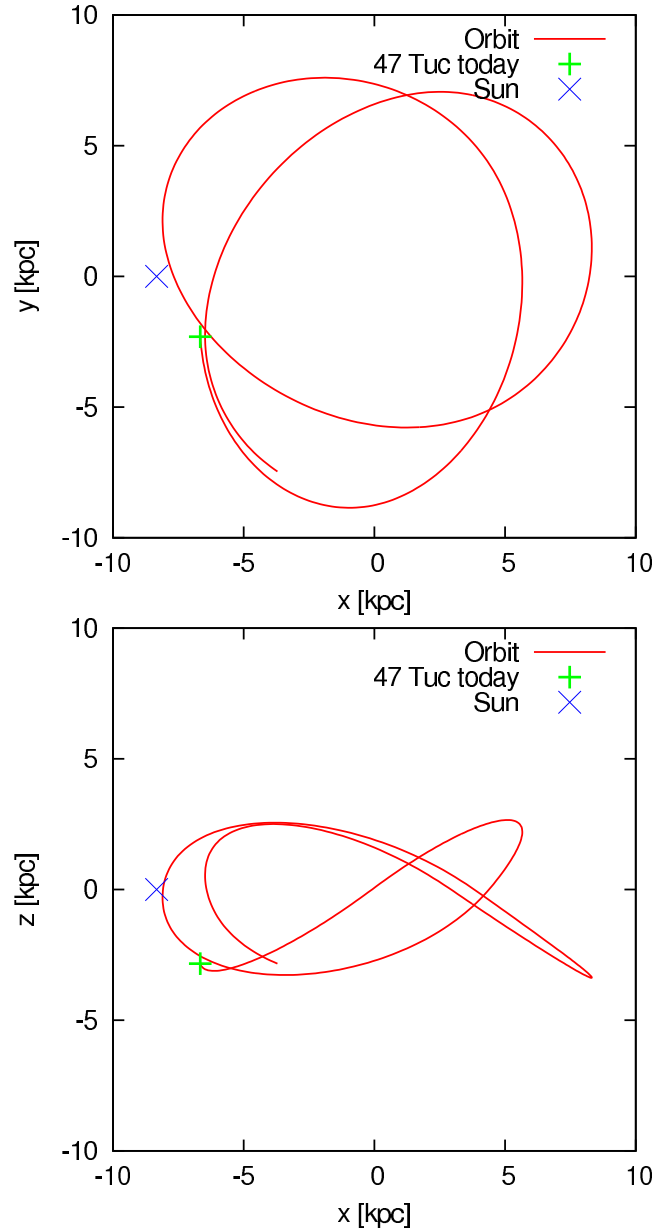


Figure 2. The orbital path of 47 Tuc from 500 Myr ago to the present time in the (x, y) plane (top panel) and in the (x, z) plane (bottom panel), based on parameters from the literature (see Table 1). The present day position of 47 Tuc is marked as a plus (+) symbol and the position of the Sun is marked as a cross (x).

potential has a circular velocity of 220 km s^{-1} at the galactocentric distance of the Sun. In total, we integrated the orbit for 1000 Myr back in time, which is the time needed to build up the tidal tails out to large angular distances from the cluster centre.

The derived orbit yields a perigalactic distance, $R_{\text{peri}} = 5.90 \text{ kpc}$ and an apogalactic distance, $R_{\text{apo}} = 9.18 \text{ kpc}$. Hence, the eccentricity, ϵ , of the orbit is

$$\epsilon = \frac{R_{\text{apo}} - R_{\text{peri}}}{R_{\text{apo}} + R_{\text{peri}}} = 0.22. \quad (1)$$

The current galactocentric distance, R_{GC} , of 47 Tuc is 7.59 kpc , and the cluster is on its way to perigalacticon. The

Table 1. Input parameters

Parameter	Value	Reference
$D_{HeliO_{47\text{ Tuc}}}$	4.02 kpc	McLaughlin et al. (2006)
$\alpha_{47\text{ Tuc}} (J2000)$	00 ^h 24 ^m 05 ^s .67	McLaughlin et al. (2006)
$\delta_{47\text{ Tuc}} (J2000)$	-72°04′52″.62	McLaughlin et al. (2006)
μ_α	5.64 mas yr ⁻¹	Anderson & King (2004)
μ_δ	-2.05 mas yr ⁻¹	Anderson & King (2004)
V_r	-16.85 km s ⁻¹	Lane et al. (2010a)
r_t	56 pc	Harris (1996); this work
M_{tot}	$1.0 \times 10^6 M_\odot$	Lane et al. (2010a); Giersz & Heggie (2011)
\dot{N}	13.9 Myr ⁻¹	Giersz & Heggie (2011)
\dot{M}	5.61 M_\odot Myr ⁻¹	Giersz & Heggie (2011)
\dot{M}/\dot{N}	0.404 M_\odot	Giersz & Heggie (2011)
$(X, Y, Z)_\odot$	(-8.3, 0.0, 0.0) kpc	Gillessen et al. (2009)
V_\odot	220.0 km s ⁻¹	Kerr & Lynden-Bell (1986)
$(U, V, W)_{\text{LSR}}$	(11.1, 12.24, 7.25) km s ⁻¹	Schönrich et al. (2010)

orbital phase, p_{orb} , as defined by Küpper et al. (2011a) is, therefore,

$$p_{orb} = \frac{\dot{R}_{GC} R_{GC} - R_{peri}}{|\dot{R}_{GC}| R_{apo} - R_{peri}} = -0.52, \quad (2)$$

which means that the cluster is half-way to perigalacticon. Its current orbital velocity is 206 km s⁻¹, while it is 160 km s⁻¹ at apogalacticon and 264 km s⁻¹ at perigalacticon. Hence, the cluster and its tails are currently being strongly accelerated.

3.2 The tidal tails

For predicting the shape and extent of the tidal tails of 47 Tuc, we apply the method introduced by Küpper, Lane & Heggie (2012). Starting at 1000 Myr in the past, we follow the orbit of 47 Tuc and calculate its theoretical tidal radius, $x_L(t)$, at time t for each timestep using

$$x_L(t) = \left(\frac{GM}{\Omega^2 - \partial^2\Phi/\partial R^2} \right)^{1/3}, \quad (3)$$

where G is the gravitational constant, M is the assumed cluster mass, Φ is the Galactic potential, Ω is the angular velocity of the cluster about the Galactic centre and R is its galactocentric distance (e.g. Heggie & Hut 2003; Küpper et al. 2010a).

Into the combined potential of the Galaxy and the cluster we inject a stream of test particles, each of which may represent an escaping star. At the time of its injection each test particle is placed at one of the two Lagrange points, L1 or L2, which lie at a distance of $\pm x_L$ from the cluster centre along the galactocentric radius vector of the cluster (the way in which the initial velocity is chosen is described below). Since the gravitational attraction of the cluster equals the repulsive forces of the effective Galactic potential at these points, the test particles can easily escape into the tidal tails of the cluster. We then integrate each released test particle to the present time, ignoring the mutual gravitational interaction between the test particles but taking the gravitational attraction of the cluster into account.

Since the tidal radius changes rapidly when the cluster goes through perigalacticon, many test particles can get recaptured on the way to apogalacticon as the tidal radius

quickly grows to its maximal value at apogalacticon. Therefore, it is no longer practical to release our test particles from the Lagrange points. Instead we introduce a minimum radius from which we release test particles, x_{edge} , which we denote the edge radius. That is, the test particles are released from a radial offset, Δx , from the cluster given by

$$\Delta x(t) = \max(x_L(t), x_{edge}). \quad (4)$$

This edge radius is found experimentally by increasing this lower limit from the perigalactic tidal radius up to the value at which no test particle is recaptured (see also Küpper, Lane & Heggie 2012, for a more detailed description). However, we will continue to use the phrase ‘‘Lagrange points’’ when referring to the points from which we release test particles.

From the results of the numerical integrations we obtain the positions of the test particles at the present time, giving streaklines such as those plotted in Fig. 3. Streaklines are a concept from fluid dynamics, in which test particles are released into a fluid from a given point to visualise flow. In engineering streaklines are often produced with smoke or dye for tracking flows of air or liquids, respectively (see Section 2.3 by Küpper, Lane & Heggie 2012, for a detailed description of the use of streaklines in the current context). Specific to the current study, we let $\mathbf{x}(t; t_0)$ be the galactocentric position at time t of a particle which was injected at time t_0 . Then a streakline in Fig. 3 is the set of points $\mathbf{x}(t; t_0)$ in which t is the present time and t_0 ranges over the duration of the simulation. Thus streaklines are not orbits. By contrast the red curve in Fig. 3 is the orbit of the cluster, the locus of its galactocentric position $\mathbf{x}(t)$, in which t ranges over the duration of the simulation. Such plots are common in work on tidal tails, e.g. Fig. 20 by Eyre & Binney (2011).

Our simulations are designed to locate the overdensities in the tidal tails of 47 Tuc caused by the epicyclic motions of the escaping stars (see Sec. 3.3). These overdensities are the direct result of the motions of the escaping stars. Escaped stars have the lowest relative motion, with respect to their neighbours, within the epicyclic loops, leading to stars ‘bunching up’ at these locations, resulting in overdensities. We performed several simulations to cover uncertainties in the cluster mass, proper motion and Heliocentric distance of the cluster. Therefore, we will first discuss a reference model,

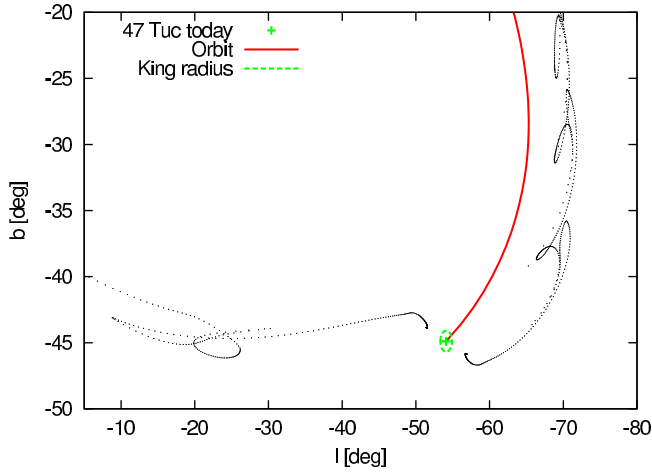


Figure 3. The final timestep (present time) of the reference model is shown. The black points are test particles. Due to the manner in which they were released from the cluster, these particles can be considered streaklines, which allow for a simple visualisation of the positions, at the present time, of stars which have escaped from 47 Tuc in the recent past. These have been produced by releasing test particles from the tidal radius of the cluster (see text). The solid red curve is the orbital path of the cluster. The current position of the cluster is marked by a green cross, and its King radius as derived from its surface density profile (see Fig. 1) is given by the green dashed curve. Escaped stars are slowest within the epicyclic loops, which is where overdensities will be visible.

then we will vary single parameters to study the effect of the changes.

Table 1 describes the parameters we have chosen for our reference model. This reference cluster has a total final mass of $1.0 \times 10^6 M_{\odot}$ and loses one star every 0.075 Myr. Its proper motion is given by $\mu_{\alpha} = 5.64 \text{ mas yr}^{-1}$ and $\mu_{\delta} = -2.05 \text{ mas yr}^{-1}$ and it has a Heliocentric distance of 4.02 kpc. We run our simulations for 1000 Myr, finishing at the present time. We have chosen 1000 Myr as this is long enough for the first, second and third order overdensities in the tidal tails to become fully populated.

In Fig. 3 the streaklines of the above setup are shown. To produce these lines we released the test particles with exactly the angular velocity of the cluster from exactly the Lagrange points (Eq. 4). The edge radius for this cluster mass was found to be 158 pc, whereas the actual tidal radius of the cluster varies between 111 pc at perigalacticon and 171 pc at apogalacticon. The epicyclic motion of the test particles in the tails is obvious. The epicyclic loops are strongly influenced and disturbed by the cluster mass.

In Fig. 4 the simulated tails of 47 Tuc are shown for two different sets of escape conditions. For the ‘warm’ escape conditions (top panel), the escaping stars retain the angular velocity of the cluster plus they obtain a random offset in velocity drawn from a Gaussian distribution with a FWHM of 1 km s^{-1} . Moreover, a Gaussian offset with a FWHM of 25% of the tidal radius has been added about the Lagrange points so that they do not all escape from a single point on the edge of the cluster. For the ‘hot’ escape conditions (bottom panel in Fig. 4) we doubled the above fluctuations, i.e. a Gaussian velocity offset with a FWHM of 2 km s^{-1} and a Gaussian spatial offset with FWHM of 50% of the

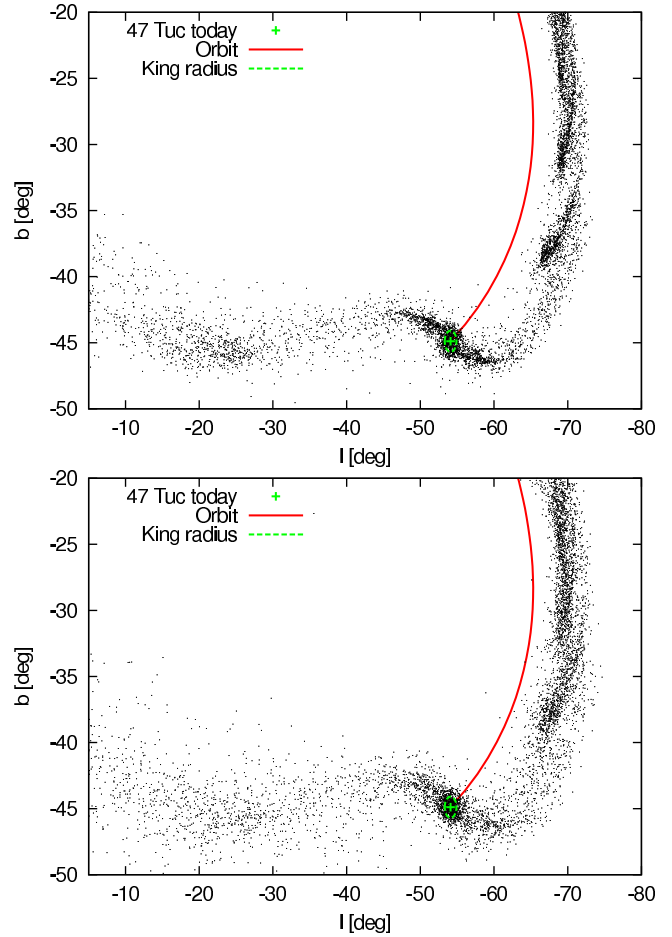


Figure 4. Same as Fig. 3, except with ‘warm’ (top panel) and ‘hot’ (bottom panel) escape conditions of the test particles (black points) as described in the text. Each test particle has been given a random spatial offset and a velocity offset at the moment of escape. Because of these offsets the test particles no longer lie along a smooth curve as in Fig. 3. The larger the spread in escape conditions, the lower the peak density within the epicyclic overdensities, however, the locations of the overdensities are only negligibly affected.

tidal radius. However, from Küpper, Lane & Heggie (2012) it is obvious that the scatter in escape conditions is in fact not very large. Hence, the ‘hot’ escape conditions can be regarded as the ‘worst case scenario’.

We see that adding random fluctuations to the escape conditions of the test particles increases the width of the tails and scatters their orbits about the ideal orbits shown in Fig. 3. The larger the scatter in escape conditions, the smaller the peak density in the epicyclic overdensities. However, the positions of the overdensities is not altered significantly.

Furthermore, we have produced several simulations to test how the uncertainty in the input parameter values affects the output of our model. For proper motion, we produce models with $\mu_{\alpha} = 4.23 \text{ mas yr}^{-1}$ and $\mu_{\delta} = 7.05 \text{ mas yr}^{-1}$ as well as with $\mu_{\delta} = -1.54 \text{ mas yr}^{-1}$ and $\mu_{\alpha} = -2.56 \text{ mas yr}^{-1}$. For our decreased and increased mass models we employ a cluster mass of $0.9 \times 10^6 M_{\odot}$ and $1.1 \times 10^6 M_{\odot}$, respectively. We also include Heliocentric dis-

tances of 4.7 kpc and 3.3 kpc because, during the writing of this paper, Woodley et al. (2012) published a Heliocentric distance of 4.7 kpc, a discrepancy of about 15% from the value we assume for our reference model. For these variations we assumed the same setup as for the ‘warm’ case mentioned above, except for the parameter which was explicitly altered. See Table 2 for a summary of the positions and peak densities of the first and second order epicyclic overdensities in the trailing tail resulting from each model. These models will be further discussed in the following section.

3.3 Epicyclic Overdensities

Despite the density of the epicyclic overdensities changing slightly from the warm to the hot escape conditions (see Models 1 and 2 in Table 2), their positions change very little, therefore, for the remainder of this paper we will mostly focus on the warm tidal tails, in the interest of brevity.

Density contours of the warm tidal tails can be seen in Figures 5 to 9. The epicyclic overdensities exhibit surface densities $\sim 3 - 4\%$ above the average Galactic background in the region near the tidal tails, depending on the model (see Table 2). Tidal features exhibiting very low surface brightness variations are recoverable using matched filtering techniques. For example, Grillmair & Johnson (2006) resolved tidal tails with extremely low surface brightness over a region of sky with a mean stellar background of $\sim 4500 \text{ deg}^{-2}$, about 50% higher than the background near the tidal overdensities of 47 Tuc. Furthermore, after applying an “optimal contrast filter” (effectively a matched filter), Odenkirchen et al. (2003) detected features with a peak $\sim 20\%$ above the background counts, and much smaller deviations from the background between the density peaks, for the tidal tails of the globular cluster Pal 5. Indeed, the authors claim that the density peaks are about twice the mean density of the tidal tails overall (i.e. the mean observed density of the tails is 10% above the background counts). Assuming their claimed 4.3 times increase in contrast using the matched filter, the density peaks for the epicyclic overdensities in the tidal tails of 47 Tuc will be $\gtrsim 13\%$ above the background, well above the detection threshold.

Furthermore, it can be seen that altering various parameters also affects the positions of the first and second order overdensities differently. This is due to the different influence of the cluster mass and the orbital phase on the appearance of the tidal tails and the overdensities (see Küpper et al. 2010a; Küpper, Lane & Heggie 2012). Hence, not only the location of the overdensities with respect to the cluster is of interest when constraining the dynamical state of the cluster, but also the relative distance between the overdensities themselves.

3.4 Comparison with N -body simulations

Figures 7-10 by Küpper, Lane & Heggie (2012) show that our formalism for releasing test particles into the tidal tails yields very good agreements with results from direct N -body simulations. However, in comparison to the models presented in that study, 47 Tuc moves on a slightly more complex orbit which also includes periodic disc crossings.

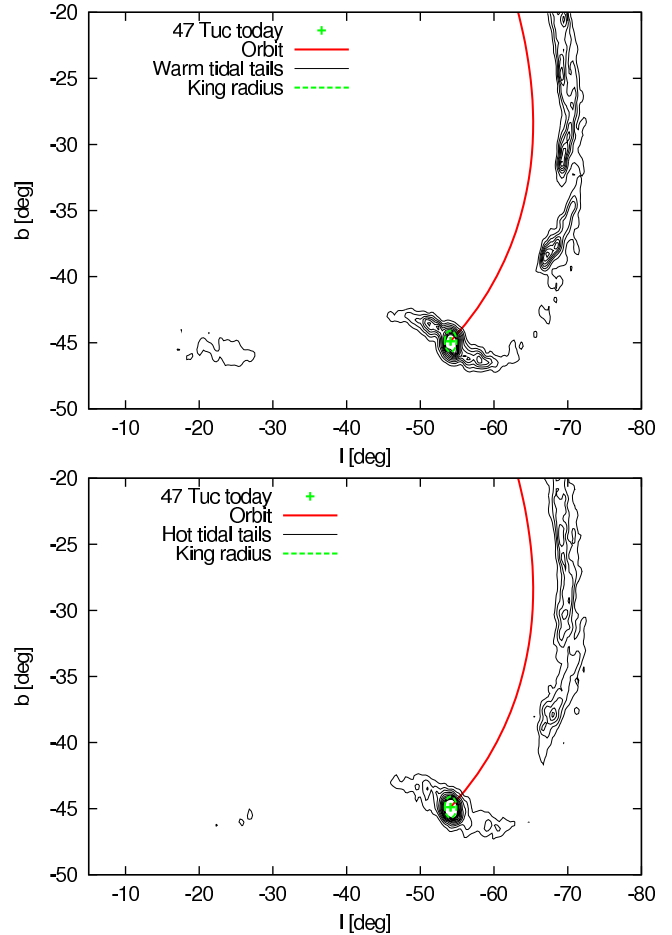


Figure 5. Contour maps of the tidal tails of 47 Tuc as shown in Fig. 4. In the top panel the warm escape conditions are shown, whereas in the bottom panel the test particles were released with hot escape conditions. The contour lines refer to 15, 30, 45, ..., stars/deg². The red solid curve is the orbital path of the cluster. The current position of the cluster is marked by a green cross, and its King radius as derived from its surface density profile (see Fig. 1) is given by the green dashed curve. As can be seen in Fig. 4, the peak density in the epicyclic overdensities gets much lower when the spread in escape conditions increases.

Depending on where a cluster crosses the Galactic disc, disc shocks can significantly heat up the cluster and increase its overall mass-loss rate (e.g. Vesperini & Heggie 1997). Furthermore, Eq. 3, which we use for calculating the distance from which we release the test particles, has to be taken as a rough approximation during these events. Therefore, we have to check if our assumptions are still valid under these conditions.

Unfortunately, a direct N -body simulation of 47 Tuc is currently not feasible due to the large number of member stars (about 2×10^6). Instead, we set up a moderately high resolution toy model of 47 Tuc with 1.1×10^5 particles using the publicly available code MCLUSTER¹ (Küpper et al. 2011b). We used a spectrum of particle masses, m , ranging from $4 - 40 M_{\odot}$ and a mass distribution proportional to

¹ www.astro.uni-bonn.de/~akuepper/mcluster/mcluster.html
www.astro.uni-bonn.de/~webaiub/german/downloads.php

Table 2. The density and Galactic coordinates of the first and second order overdensities, the proper motion, final (present day) cluster mass, Heliocentric distance and escape conditions for each of our models. Only the trailing tail is represented here for brevity. Information is for the peak density in each overdensity only. Note that the approximate average density of the stellar background in the regions of the first and second tidal overdensities is 3000 stars per square degree, based on 2MASS point sources.

Model	Σ_1 ★/deg ²	Σ_2 ★/deg ²	(l,b) ₁ deg	(l,b) ₂ deg	μ_α mas yr ⁻¹	μ_δ mas yr ⁻¹	$\times 10^6$ M _⊙	D kpc	Esc
1	105	90	(-67.2,-38.3)	(-69.2,-31.3)	5.64	-2.05	1.0	4.02	warm
2	70	55	(-68.0,-37.9)	(-69.6,-30.3)	5.64	-2.05	1.0	4.02	hot
3	105	90	(-67.4,-37.7)	(-68.2,-30.8)	7.05	-2.05	1.0	4.02	warm
4	115	115	(-68.5,-38.0)	(-69.7,-31.0)	4.23	-2.05	1.0	4.02	warm
5	105	95	(-66.9,-39.7)	(-69.2,-33.6)	5.64	-2.56	1.0	4.02	warm
6	115	110	(-67.5,-37.0)	(-69.4,-29.0)	5.64	-1.54	1.0	4.02	warm
7	100	90	(-67.6,-38.1)	(-69.5,-30.9)	5.64	-2.05	1.1	4.02	warm
8	110	95	(-67.0,-38.5)	(-69.2,-31.7)	5.64	-2.05	0.9	4.02	warm
9	105	100	(-69.7,-36.0)	(-71.3,-26.6)	5.64	-2.05	1.0	3.30	warm
10	130	110	(-65.4,-39.8)	(-67.7,-33.8)	5.64	-2.05	1.0	4.70	warm

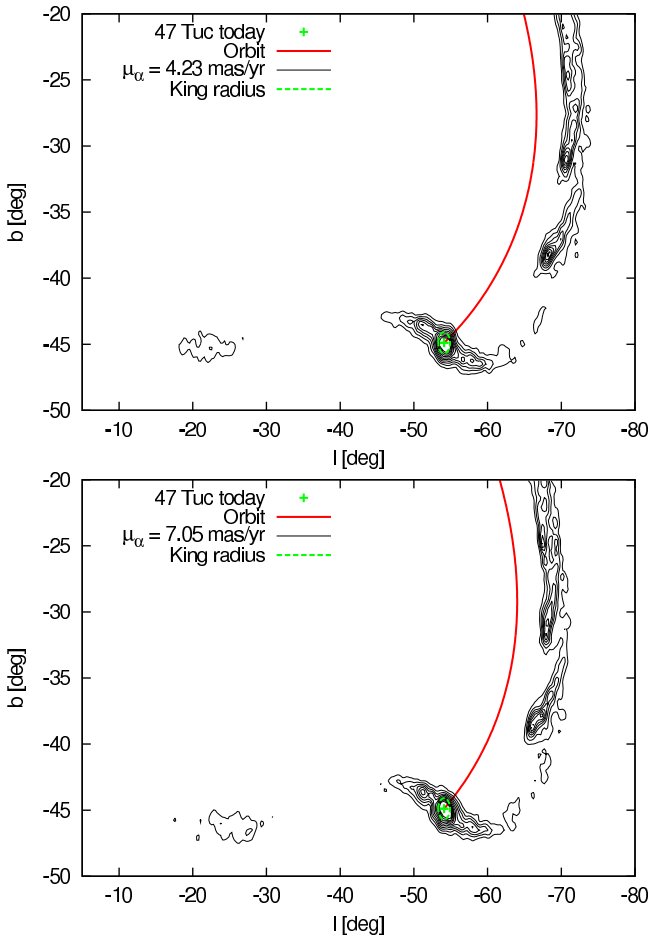


Figure 6. Same as for the top panel of Fig. 5, except with $\mu_\alpha = 4.23 \text{ mas yr}^{-1}$ (top panel) and $\mu_\alpha = 7.05 \text{ mas yr}^{-1}$ (bottom panel).

$m^{-2.35}$, adding up to a total mass of $1.0 \times 10^6 M_\odot$. The particles were distributed in a Plummer (1911) sphere with a half-mass radius of 10 pc, largely consistent with the surface density profile of 47 Tuc. The cluster was integrated along the orbit of 47 Tuc for 1 Gyr using NBODY6 (Aarseth 2003) on a GPU computer at AIfA Bonn. Over the course of the simulation the cluster model lost about 3% of its mass into

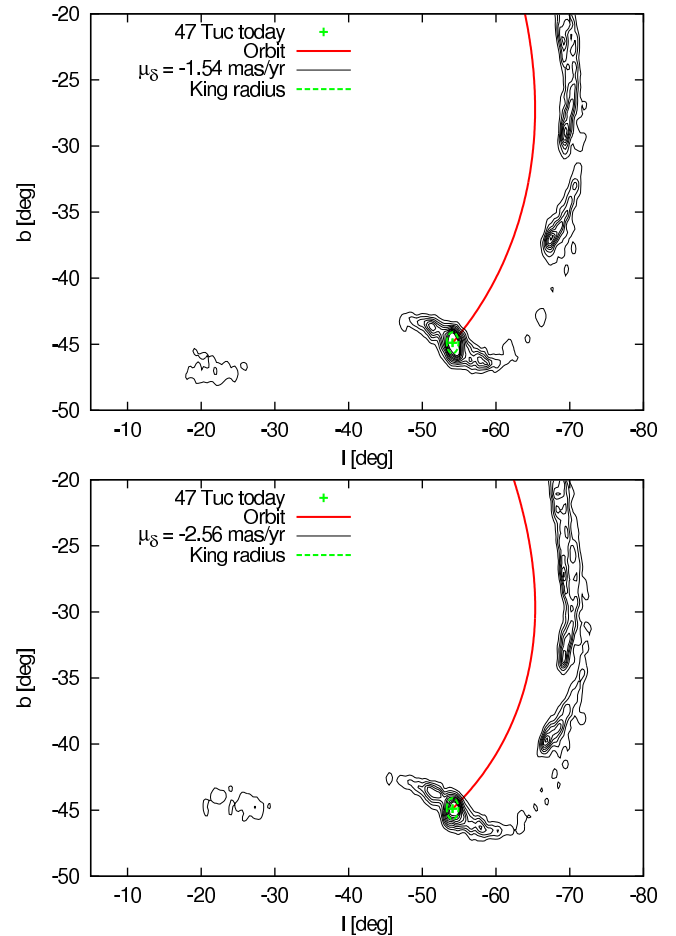


Figure 7. Same as for the top panel of Fig. 5, except with $\mu_\delta = -1.54 \text{ mas yr}^{-1}$ (top panel) and $\mu_\delta = -2.56 \text{ mas yr}^{-1}$ (bottom panel).

the tidal tails such that its final mass resembles the present-day mass of 47 Tuc, within observational uncertainties.

In Fig. 10 the cluster and its tails are shown after the integration. Given the simplicity of our N -body model, the distribution of particles in the tails resembles our predictions from the streakline models very well (*cf.* Figs. 4 & 5). The overall shape and the positions of the overdensities matches

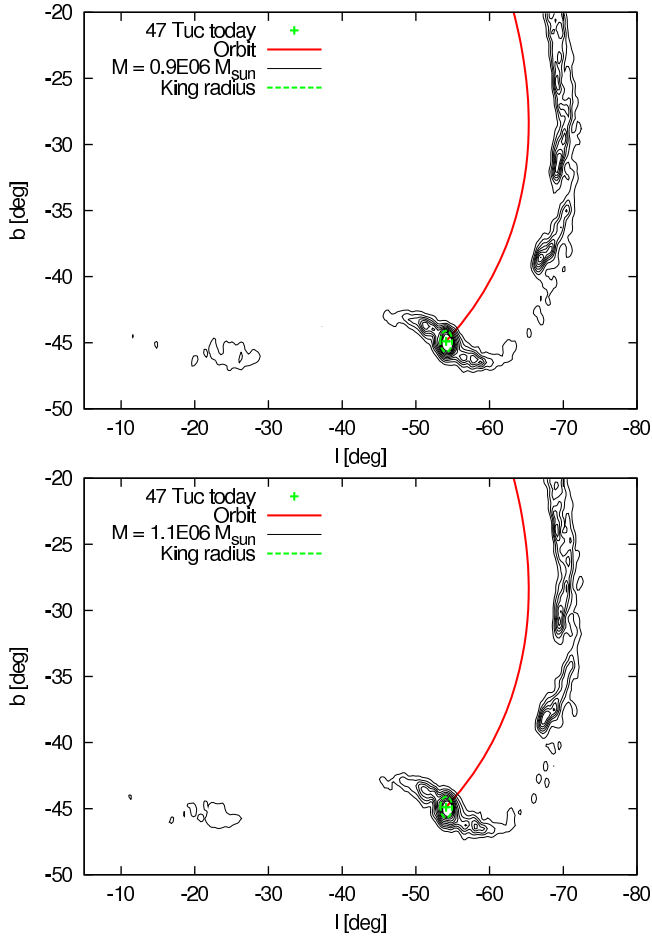


Figure 8. Same as for the top panel of Fig. 5, except with $M = 0.9 \times 10^6 M_{\odot}$ (top panel) and $M = 1.1 \times 10^6 M_{\odot}$ (bottom panel).

the predictions from the ‘hot’ escape conditions best. However, a more realistic simulation with ~ 20 times the number of particles would have a longer relaxation time and, therefore, its mass-loss rate would differ from that of our model. Hence, the particle density in this simulation cannot be taken as direct proxy for the expected stellar density. Moreover, a simulation with 2×10^6 particles would exhibit much less scatter in escape conditions and, therefore, dynamically colder tidal tails (see Küpper et al. 2008). Thus, we expect that the tidal tails of 47 Tuc rather resemble the ‘warm’ escape conditions.

Our simplified model (Section 3.2) assumes that the injection rate is constant, however, in the N -body model described in the current Section, the Galactic potential includes a disc component. This may, in principle, modulate the escape rate via disc shocking. However, this simulation demonstrates that disc shocks do not significantly affect the shape of the tidal tails or the positions of the epicyclic overdensities within them. Furthermore, while it is true that the additional energy input from tidal shocks, which is distributed within the cluster, results in a higher average mass loss rate, it was estimated by Aguilar et al. (1988) that such shocks only contribute $\sim 1\%$ to the total destruction rate. Moreover, this increase in mass loss is distributed nearly homogeneously over the whole orbit because the escape of the stars is delayed until well after the disc shock, often for sev-

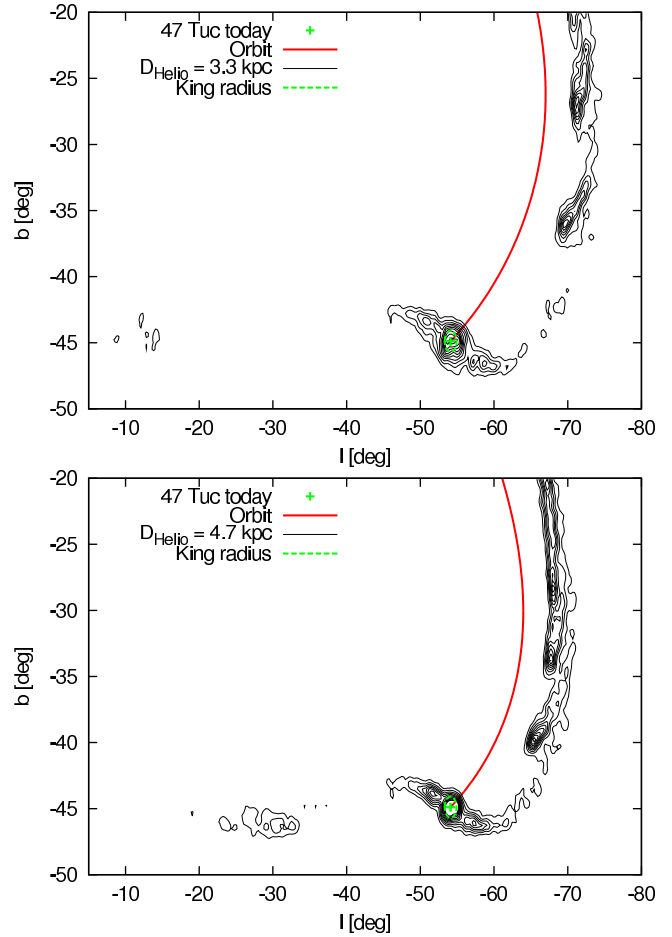


Figure 9. Same as for the top panel of Fig. 5, except with $D_{\text{helio}} = 3.3 \text{ kpc}$ (top panel) and $D_{\text{helio}} = 4.7 \text{ kpc}$ (bottom panel).

eral orbits of the star within the cluster, even for clusters on non-circular orbits (Küpper et al. 2010a). This delay is the result of the stars preferentially leaving the system through the Lagrange points, where the potential barrier is at its minimum. Stars excited to escape energies by shocks leave the cluster on about the same time-scale as due to other evaporative processes, and may even stay bound to the cluster for as long as a Hubble time (Fukushige & Heggie 2000), at least for clusters on circular orbits. The energetically unbound stars enhancing the outer velocity dispersion of 47 Tuc (Lane et al. 2010a) also support the concept of delayed escape, especially if these unbound stars were excited during the last disc passage which, from our simulations, occurred about 70 Myr ago. Therefore, because energetically unbound stars cannot all escape immediately following shocks, and can stay bound to the cluster for long periods, we do not expect to see additional substructure in the tidal tails caused by disc crossings.

While we used the analytic potential suggested by Allen & Santillan (1991) for the streakline models as well as for the N -body model, Dehnen & Binney (1998) argue that the Galactic disc structure is actually more complex than the single-component exponential disc used by Allen & Santillan. However, the strongest disc shock 47 Tuc experiences is at 6 kpc. At this distance the two potentials do

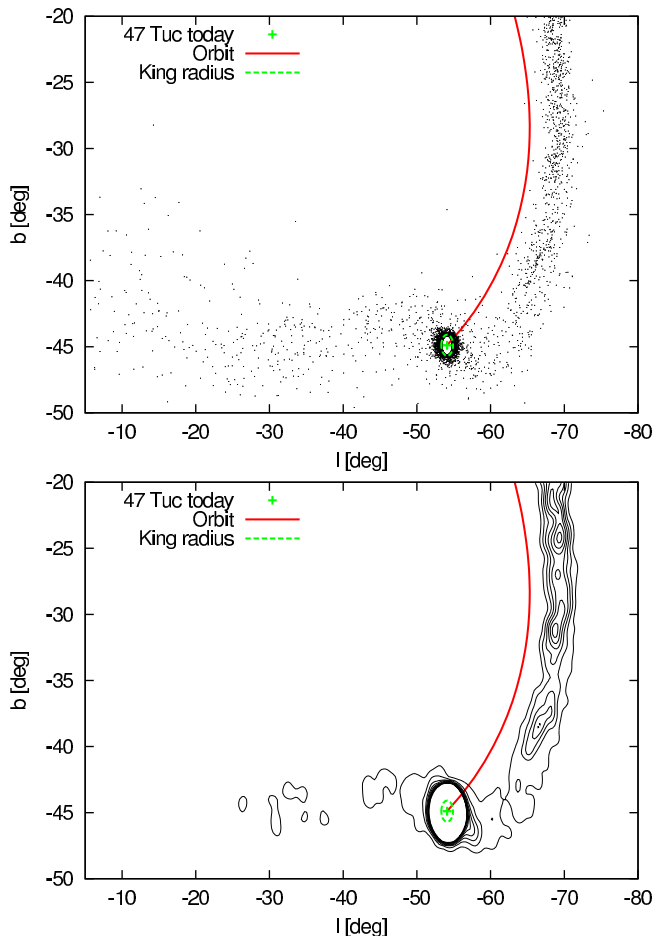


Figure 10. Distribution of tail stars from a simple N -body simulation. The shape of the tails and the positions of the overdensities agree very well with the predictions from our streakline models. A more realistic N -body model with a larger number of particles (here we use 110 000) will show less scatter in escape conditions and will result in dynamically colder tidal tails (see Sec. 3.4). Particles within the King radius are not shown in the upper panel for clarity. The contour lines in the lower panel refer to 2.5, 5, 7.5, ..., particles per square degree. Due to the smaller number of particles in the tidal tails we used a Gaussian smoothing kernel with FWHM = 1° , twice as large as for our other contour plots (Figs. 5-9).

not differ greatly (e.g. Kaempf, de Boer & Altmann 2005; Jilková et al. 2012). Therefore, we do not expect our predictions to be significantly affected by the stronger disc shocking suggested by Dehnen & Binney (1998).

4 CONCLUSIONS

We have employed the most accurate available data on the Milky Way globular cluster 47 Tuc to compute its orbit about the Galaxy. Moreover, we used the streakline method (Küpper, Lane & Heggie 2012) to predict the shape of the tidal tails of 47 Tuc and the locations of the epicyclic overdensities within those tails. By varying the input parameters of our models we show how the most important input values influence the locations and peak surface densities of the epicyclic overdensities.

We find that the epicyclic overdensities exhibit peak surface densities $\sim 3 - 4\%$ above the Galactic background. These should be observationally detectable, assuming a matched filter, or similar analysis technique, is used.

Clearly variations in Heliocentric distance and proper motion alter the positions of the tidal overdensities more than variations in any other parameter in our model. Our variations in proper motion are much larger than the observational error stated by Anderson & King (2004) and we find only a small change in the position of the overdensities. However, determining the distance to 47 Tuc is an ongoing problem, with many different estimates published over many years (see Gratton et al. 2003, for several examples). Therefore, finding these overdensities observationally will not only provide further constraints on the proper motion of the cluster, but will also constrain the other dynamical characteristics, including, importantly, the Heliocentric distance.

In addition, uncovering these overdensities observationally may reinforce our understanding of Newtonian gravity. While it is not within the scope of the current paper to make predictions regarding the tidal tails and their overdensities in modified gravity environments, it would be extremely interesting to see the morphology of the tidal tails as predicted by modified gravitational theories, since we would expect them to differ significantly from our predictions.

Finally, our study has shown how, in principle, the shape and extent of the tidal tails of any star cluster can be quickly predicted without requiring extensive N -body simulations. This will be especially helpful for large parameter studies or for massive star clusters which cannot be addressed by means of direct N -body computations due to hardware limitations.

ACKNOWLEDGMENTS

R.R.L. gratefully acknowledges support from the Chilean Center for Astrophysics, FONDAF No. 15010003. A.H.W.K. kindly acknowledges support by the ESO Director General Discretionary Fund and the German Research Foundation (DFG) project KR 1635/28-1.

Many thanks go to László Kiss for the use of the data that went into this publication, including velocities extracted from the raw spectra.

We would like to thank the anonymous referee for many useful comments.

REFERENCES

- Aarseth, S. J. 2003, *Gravitational N-Body Simulations*, by Sverre J. Aarseth, pp. 430. ISBN 0521432723. Cambridge, UK: Cambridge University Press, November 2003
- Aguilar, L., Hut, P., & Ostriker, J. P. 1988, *ApJ*, 335, 720
- Allen C., Santillan A., 1991, *RMxAA*, 22, 255
- Anderson J., King I. R., 2004, *AJ*, 128, 950
- Dehnen W., Binney J., 1998, *MNRAS*, 294, 429
- Drukier G. A., Slavin S. D., Cohn H. N., Lugger P. M., Berrington R. C., Murphy B. W., Seitzer P. O., 1998, *AJ*, 115, 708
- Eyre, A., & Binney, J. 2011, *MNRAS*, 413, 1852
- Fukushige T., Heggie D. C., 2000, *MNRAS*, 318, 753

- Giersz M., Heggie D. C., 2011, MNRAS, 410, 2698
- Gillessen S., Eisenhauer F., Trippe S., Alexander T., Genzel R., Martins F., Ott T., 2009, ApJ, 692, 1075
- Gratton R. G., Bragaglia A., Carretta E., Clementini G., Desidera S., Grundahl F., Lucatello S., 2003, A&A, 408, 529
- Grillmair C. J., Johnson R., 2006, ApJ, 639, L17
- Harris W. E., 1996, AJ, 112, 1487
- Heggie D., Hut P., 2003, *The Gravitational Million-Body Problem*, Cambridge, UK, Cambridge University Press
- Jílková, L., Carraro, G., Jungwiert, B., & Minchev, I. 2012, *Assembling the Puzzle of the Milky Way*, Le Grand-Bornand, France, Edited by C. Reylé; A. Robin; M. Schultheis; EPJ Web of Conferences, Volume 19, id.07005, 19, 7005
- Just A., Berczik P., Petrov M. I., Ernst A., 2009, MNRAS, 392, 969
- Kaempf T. A., de Boer K. S., Altmann M., 2005, A&A, 432, 879
- Kerr F. J., Lynden-Bell D., 1986, MNRAS, 221, 1023
- King I., 1962, AJ, 67, 471
- Kiss L. L., Székely P., Bedding T. R., Bakos G. Á., Lewis G. F., 2007, ApJL, 659, L129
- Koposov S. E., Rix H.-W., Hogg D. W., 2010, ApJ, 712, 260
- Küpper A. H. W., MacLeod A., Heggie D. C., 2008, MNRAS, 387, 1248
- Küpper A. H. W., Kroupa P., Baumgardt H., Heggie D. C., 2010a, MNRAS, 401, 105
- Küpper A. H. W., Kroupa P., Baumgardt H., Heggie D. C., 2010b, MNRAS, 407, 2241
- Küpper A. H. W., Mieske S., Kroupa P., 2011a, MNRAS, 413, 863
- Küpper A. H. W., Maschberger T., Kroupa P., Baumgardt H., 2011b, MNRAS, 417, 2300
- Küpper A. H. W., Lane R. R., Heggie D. C., 2012, MNRAS, 420, 2700
- Lane R. R., Kiss L. L., Lewis G. F., Ibata R. A., Siebert A., Bedding T. R., Székely P., 2010a, MNRAS, 401, 2521
- Lane R. R., et al., 2010b, ApJL, 711, L122
- McLaughlin D. E., Anderson J., Meylan G., Gebhardt K., Pryor C., Minniti D., Phinney S., 2006, ApJS, 166, 249
- Odenkirchen M., et al., 2003, AJ, 126, 2385
- Plummer, H. C. 1911, MNRAS, 71, 460
- Reid M. J., Brunthaler A., 2004, ApJ, 616, 872
- Scarpa R., Falomo R., 2010, A&A, 523, A43
- Schönrich R., Binney J., Dehnen W., 2010, MNRAS, 403, 1829
- Skrutskie M. F., et al., 2006, AJ, 131, 1163
- Steinmetz M., et al., 2006, AJ, 132, 1645
- Vesperini, E., & Heggie, D. C. 1997, MNRAS, 289, 898
- Woodley, K. A., Goldsbury, R., Kalirai, J. S., et al. 2012, AJ, 143, 50
- Zwitter T., et al., 2008, AJ, 136, 4211

This paper has been typeset from a \LaTeX file prepared by the author.